Letter | Editors' Suggestion

Exotic magnetic and electronic properties of layered CrI_3 single crystals under high pressure

Anirudha Ghosh,[1] D. Singh,[1] T. Aramaki,[2] Qingge Mu,[3] V. Borisov,[1] Y. Kvashnin,[1] G. Haider,[4] M. Jonak,[5] D. Chareev,[6,7,8] S. A. Medvedev,[3] R. Klingeler,[5] M. Mito,[2] E. H. Abdul-Hafidh,[9] J. Vejpravova,[10] M. Kalbàč,[4] R. Ahuja,[1] Olle Eriksson,[1,11] and Mahmoud Abdel-Hafiez[1,*]

[1]*Department of Physics and Astronomy, Uppsala University, Box 516, SE-751 20 Uppsala, Sweden*
[2]*Graduate School of Engineering, Kyushu Institute of Technology, Fukuoka 804-8550, Japan*
[3]*Max Planck Institute for Chemical Physics of Solids, D-01187 Dresden, Germany*
[4]*J. Heyrovsky Institute of Physical Chemistry of the Czech Academy of Sciences, Dolejškova 2155, 182 23 Prague, Czech Republic*
[5]*Kirchhoff Institute of Physics, Heidelberg University, 69120-Heidelberg, Germany*
[6]*National University of Science and Technology "MISiS," Moscow 119049, Russia*
[7]*Institute of Experimental Mineralogy (IEM RAS), Chernogolovka, Moscow Region 142432, Russia*
[8]*Ural Federal University, Ekaterinburg 620002, Russia*
[9]*Physics Department, Faculty of Science at Taibah University-Yanbu, King Khalid Road, Al Amoedi, 46423, Yanbu El-Bahr 51000, Saudi Arabia*
[10]*Department of Condensed Matter Physics, Faculty of Mathematics and Physics, Charles University, Ke Karlovu 5, 121 16 Prague 2, Czech Republic*
[11]*School of Science and Technology, Örebro University, SE-701 82 Örebro, Sweden*

(Received 8 April 2021; revised 16 November 2021; accepted 25 January 2022; published 8 February 2022)

Through advanced experimental techniques on CrI_3 single crystals, we derive a pressure-temperature phase diagram. We find that T_c increases to ∼66 K with pressure up to ∼3 GPa followed by a decrease to ∼10 K at 21.2 GPa. The experimental results are reproduced by theoretical calculations based on density functional theory where electron-electron interactions are treated by a static on-site Hubbard U on Cr $3d$ orbitals. The origin of the pressure-induced reduction of the ordering temperature is associated with a decrease in the calculated bond angle, from 95° at ambient pressure to ∼85° at 25 GPa. Above 22 GPa, experiment and theory jointly point to the idea that the ferromagnetically ordered state is destroyed, giving rise first to a complex, unknown magnetic configuration, and at sufficiently high pressures a pure antiferromagnetic configuration. This sequence of transitions in the magnetism is accompanied by a well-detected pressure-induced semiconductor-to-metal phase transition that is revealed by both high-pressure resistivity measurements and *ab initio* theory.

DOI: 10.1103/PhysRevB.105.L081104

Two-dimensional (2D) van der Waals (vdW) materials offer a plethora of functional properties that are not only of fundamental interest but also essential for the development of new technological applications [1–3]. Layered chromium trihalides emerged as potential 2D vdW materials with unique layer-dependent magnetic properties [4,5]. Understanding the long-range magnetic order in these 2D materials is an intriguing subject of widespread research. According to the Mermin-Wagner theorem [6], it is strongly suppressed in a 2D isotropic Heisenberg system due to spin fluctuations at any finite temperature. Here, the magnetocrystalline anisotropy (MCA) comes to the rescue and stabilizes the long-range magnetic order in CrI_3 [7–11]. Several experiments and theories have been put forward, reflecting the role of I-5p state spin-orbit coupling (SOC) strength in the origin of the MCA through the Cr-3d–I-5p–Cr-3d superexchange interaction. This interaction is mediated by I ions octahedrally coordinating with Cr ions with an in-plane Cr-I-Cr bond angle of 95°. According to the Goodenough-Kanamori-Anderson (GKA) rule, the magnetic interaction is primarily ferromagnetic (FM) when the metal-ligand-metal bond angle is 90° [12]. Therefore the Cr-I-Cr bond angle plays a significant role in understanding the long-range FM superexchange interaction [13], as well as the MCA. Further modification in the bond angle should have a substantial impact on the electronic, magnetic, and transport properties of CrI_3. Theoretical calculations of a favorable magnetic ground state in monolayer CrI_3 are not too conclusive, as they suggest both FM [14] and antiferromagnetic (AFM) [13] ground states under lattice compression. However, a more recent calculation suggests that depending on the anisotropy of the in-plane lattice strains, both these ground states can coexist with a possibility of a complete quenching of the magnetic order at a critical isotropic lattice compression [15]. Experimentally, an increase in the FM T_c with pressure was attributed to a possible decrease in the Cr-I-Cr bond angle towards 90° [16]. However, with a maximum pressure of only 1 GPa, the variation of T_c in a broader range of pressures eluded experimental detection. This prohibits an experimental analysis of the possible decrease in the Cr-I-Cr bond angle below 90°, and its influence on the strength of the Cr-Cr superexchange interaction and T_c.

The experiments reported here go up to ∼40 GPa and offer possibilities to tune the T_c, phonon dispersions, and electronic, magnetic, and magnetotransport properties of

*mahmoud.hafiez@physics.uu.se

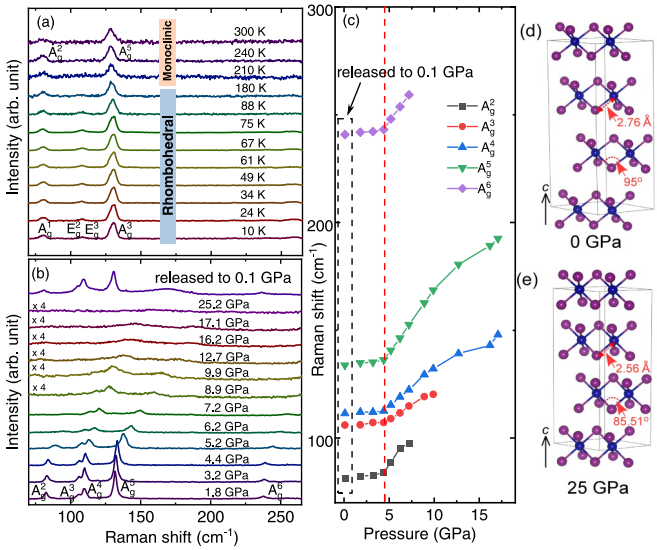

FIG. 1. (a) Temperature-dependent Raman spectra measured with circularly polarized light in parallel polarization configuration (see Supplemental Material for detailed analysis). (b) Pressure-dependent Raman spectra at 300 K measured at parallel polarization configuration. (c) Raman shift of all the phonon modes with pressure obtained from the spectra presented in (b). The red dashed line shows the pressure above which blueshift and smearing of peaks occur. Calculated structure (d) at 0 GPa and (e) at 25 GPa.

CrI_3 single crystals. Overall, understanding the correlation between the bond angle and various magnetic and electronic properties is questionable and elusive. Here, we provide a comprehensive answer to this question for CrI_3 through combined complementary experimental and theoretical studies (see Supplemental Material for details [17]; also see Refs. [18–45] therein). We observe pressure-induced semiconductor-to-metal (SM) and FM-to-AFM phase transitions. Temperature-dependent Raman spectra at ambient pressure show a FM-to-paramagnetic (T_c) transition and a rhombohedral-($R\bar{3}$)-to-monoclinic-($C2/m$) structural (T_s) transition at ∼60 K and ∼210 K [46], respectively [see Fig. 1(a), and for detailed analysis of the Raman experiment, see Supplemental Material [17]]. The obtained ambient pressure Raman spectra are in excellent agreement with theoretically obtained spectra of perfect crystals, suggesting a high crystalline purity of the synthesized material [47–49]. The pressure-dependent Raman spectra reported here [see Fig. 1(b)] present only small variation in the optical phonon frequencies up to 4.4 GPa. Above 4.4 GPa, in Fig. 1(c), a sizable blueshift with a significant decrease in intensities of all the optical phonon frequencies is observed. Additionally, above this pressure, the distinctive phonon spectral features begin to smear out into broad features, and the A_g^2 and A_g^6 phonon modes are gradually suppressed and disappear above 7.2 GPa. Above 17.1 GPa, the rest of all the phonon modes are suppressed, which is indicative of a pressure-induced deformation or distortion of the lattice. The phonon modes reappear when the pressure is released to near-ambient conditions. However, a broad feature near 175 cm^{-1} appears when pressure is released to 0.1 GPa, which is reminiscent of a high-pressure phase and suggests that the structural distortions in the pressure cycle are not perfectly reversible [17]. The broadening and suppression of the vibration modes might be indicative of modulation in the Cr-I-Cr bond angle as well as an indication towards metallization. Our density functional theory (DFT) calculations reported here do, however, show a distinct decrease in the bond angle and Cr-I bond length with pressure [see Figs. 1(d) and 1(e)] without any indication of structural transition (see Fig. S6) [17].

The optimized lattice parameters at zero pressure are calculated from DFT to be $a = b = 6.886$ Å and $c = 19.820$ Å, which are consistent with the previous results [46]. Since the FM superexchange interaction strength is associated with the Cr-I-Cr bond angle, a modification in the same is expected to influence the magnetic properties. To analyze this further, we have carried out magnetization experiments at various external pressures. At ambient conditions, Fig. 2(a) shows no frequency-dependent shift in the T_c for χ', signifying a non-spin-glass behavior [50]. Figures 2(b)–2(d) summarize the variation of the real part of ac magnetization with pressure up to 16.1 GPa and its first derivative (dm'/dT in Fig. 2(c) upto 7.2 GPa). T_c of two samples (S1 and S2 prepared at different batches) is obtained from the peaks of the Gaussian fit of the dm'/dT plots and are plotted in Fig. 2(e). An increase in broadening of the Gaussian-shaped peaks in Fig. 2(c) with pressure illustrates that the phase transition is much less distinct with atomic moments that disorder over a much wider temperature range. The Gaussian peaks in Fig. 2(d) are too broad to estimate above 7.2 GPa. The sample, however, nearly recovered to the magnetic state at ambient pressure after being released from 16 GPa, as shown in Fig. 2(f). This magnetic recovery is consistent with that of the recovery in the phonon modes, shown in Fig. 1(b). The overall variation in T_c can be attributed to the change in the Cr-I-Cr superexchange interaction owing to a variation in the Cr-I-Cr bond angle with pressure as shown in Figs. 1(d) and 1(e). In agreement with the observed variation of T_c, our theoretical studies of the crystal structure imply a decrease in the bond angle below 90° for pressures higher than 4 GPa. The calculated bond angle is about 90° at 4 GPa, close to the pressure where T_c is maximum, which is in agreement with the Goodenough-Kanamori rule [12]. From the general line shape of m' data in Fig. 2(b) [51], it is evident that a magnetically ordered state is the ground state up to the maximum measured pressure of 7.2 GPa. This is partially consistent with earlier theoretical calculations where a FM ground state was predicted even at a high compressive lattice strain [14].

To understand the magnetotransport properties and the fate of magnetic ordering at high pressures beyond the numerous studies in magnetoresistance (MR) [52,53], we have carried out MR measurements at different high pressures. Figures 3(a)–3(c) illustrate the field-dependent MR at various temperatures and 21.2, 24.0, and 37.8 GPa, respectively. A negative MR can be explained as a consequence of suppressed spin-spin scattering in a FM ordered state [54], and we associate, in fact, a negative MR as a sign of ferromagnetic ordering. Since the current is applied along the sample plane, the incoming electrons' spin will always experience a lattice with parallel spin configuration (due to intralayer ferromagnetism) below T_c. The MR can increase and be positive if the in-plane spins in the lattice are disordered (i.e., not primarily

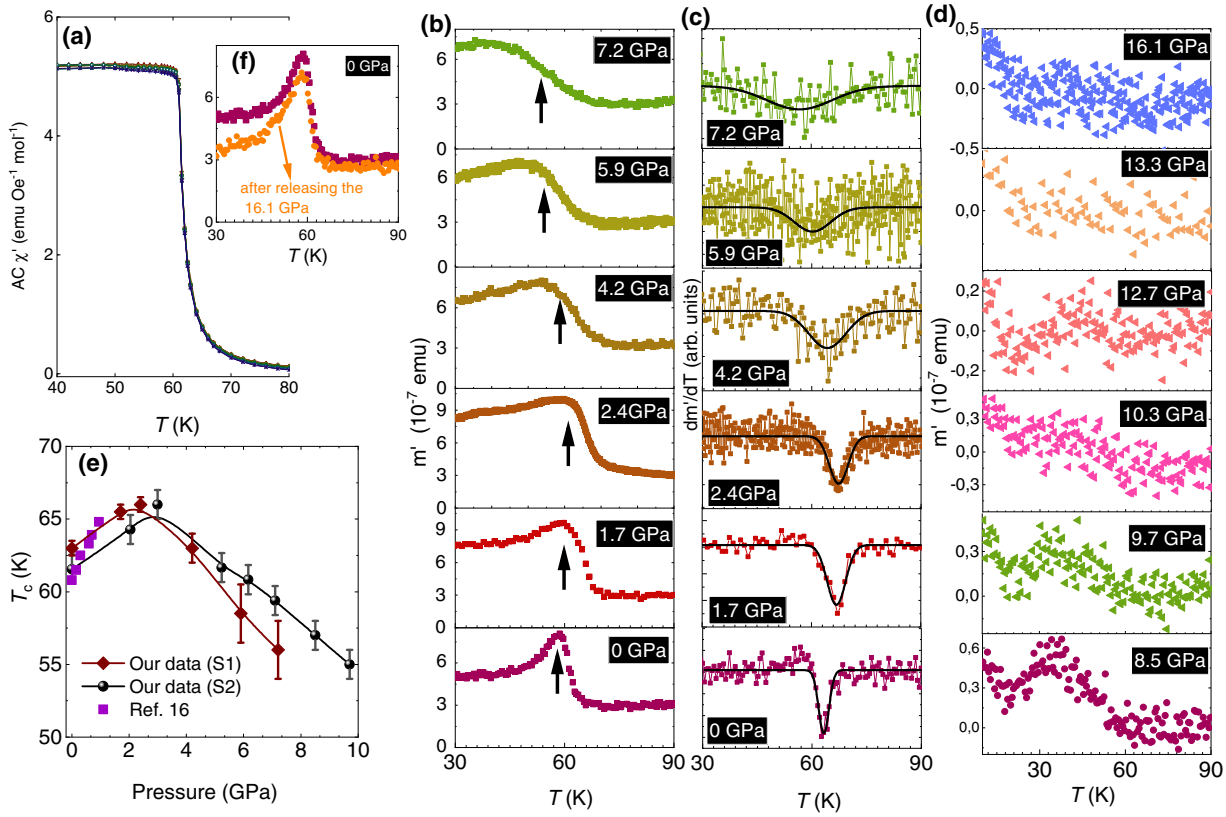

FIG. 2. (a) Frequency dependence between, 500 Hz - 10 kHz, of the real part of ac susceptibility at a magnetic field of $H_{AC} = 2$ Oe. (b) Pressure-dependent real part of the ac susceptibility plots at a magnetic field of $H_{AC} = 3.86$ Oe oscillating at a frequency of $f = 10$ Hz in crystal S2. (c) dm'/dT plot of the data shown in (b), stacked over one another for clarity. Solid black lines represent the Gaussian fit to find the minimum, which represents T_c and is in agreement with the arrows in (b). (d) Pressure-dependent real part of the ac susceptibility plots [continuation of (b)] at higher pressures, up to 16.1 GPa. (e) Plot of T_c, where the error bars represent the computational error in the Gaussian fit. Data points from Ref. [16] are shown for comparison. (f) Temperature dependence of AC χ' at initial 0 GPa and 0 GPa after releasing the maximum applied pressure of 16.1 GPa.

FM) or ordered antiferromagnetically [55]. At 21.2 GPa, the MR is negative and saturates at high magnetic fields and temperatures below 20 K [Fig. 3(a)], with the minimum at 10 K. We take this as a sign that at this pressure the onset of the FM ordered state should lie near 10 K. At 24 GPa [Fig. 3(b)] a more complex behavior is seen: The MR is seen to not saturate even down to the lowest measured temperature. In addition, for the low-temperature curves there is an initial negative downturn with applied field followed by an upturn and positive MR. This indicates a more complex magnetic state that shows signals of the MR that are not typical for either FM or AFM ordered states [55]. As we shall see below and in the Supplemental Material [17], when discussing the theoretical data, this experimental observation is consistent with a complex magnetic state, possibly a self-induced spin glass [56]. At high pressures, e.g., 37.8 GPa [Fig. 3(c)], the MR is positive for all field strengths and all temperatures. Together with the theoretical calculations, described below and in the Supplemental Material, this suggests an AFM state, which increases with decrease in temperature (inverse temperature dependence of positive MR) [55]. Note that a positive, nonsaturating MR, even at 9 T magnetic field, could stem from an enhanced spin-spin scattering due to the disordered spins or a more complex spin structure. However, as the theoretical results show below, a pure AFM state is the most likely scenario.

It is evident from our calculations that the in-plane Cr-Cr interactions are AFM for pressures above 30 GPa (Fig. S6). This is not inconsistent with what is known at ambient conditions; Cr-Cr interactions of strained monolayer CrI_3 are AFM [15]. However, in our calculations at 10 and 20 GPa, the nearest- and next-nearest-neighbor Cr-Cr interactions for bulk CrI_3 are FM and AFM, respectively, while at zero pressure both interactions are FM, consistent with the measured ground state of bulk CrI_3 [57]. Between 20 and 30 GPa, however, our first-principles results suggest that there can be a competition between the intralayer and interlayer interactions, which are both FM and AFM, and this may lead to more complex magnetic phases than collinear FM and AFM states observed in chromium trihalides at zero pressure. Therefore it is clear that the pressure-induced FM-to-AFM crossover is most likely to occur above 30 GPa. Our present results show the emergence of a magnetically complex state in the region just above 22 GPa. This pressure is equivalent to an isotropic compressive lattice strain of 14% as compared with 5% in monolayer CrI_3 [15]. Furthermore, in Fig. 3(d), our data show a change in the slope of the resistivity curves above 21.2 GPa, which resembles a transition to a metallic state above

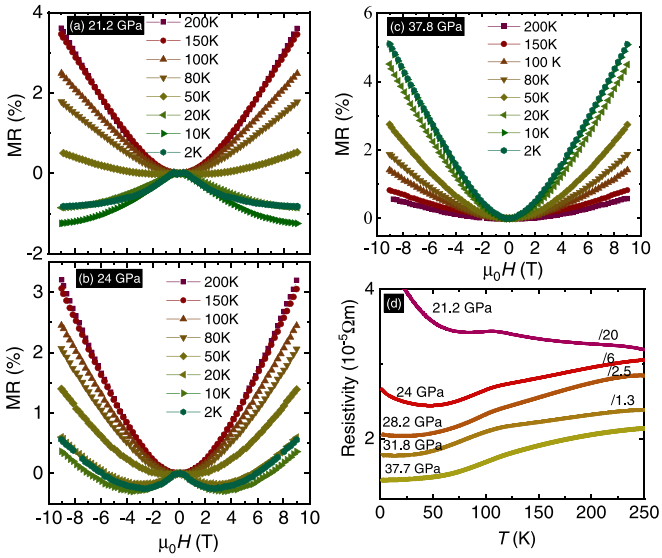

FIG. 3. Field-dependent MR under 21.2 GPa (a), 24 GPa (b), and 37.8 GPa (c). (d) Temperature-dependent resistivity at high pressure, illustrating a semiconductor-to-metal transition above 21.2 GPa.

21.2 GPa, in agreement with the pressure-induced broadening of Raman peaks in Fig. 1(b) that we interpret is due to metallization. These measurements reveal that the quenching of magnetic ordering concurrently evolves in the metallic state.

The spin-polarized calculations corroborate with the SM transition. In Fig. 4(a) it can been seen that the conduction band minimum is composed of spin-polarized up-spin channels of Cr-3d and I-5p states. It can be seen that the band gap mainly originates between the I-5p state in the valence band

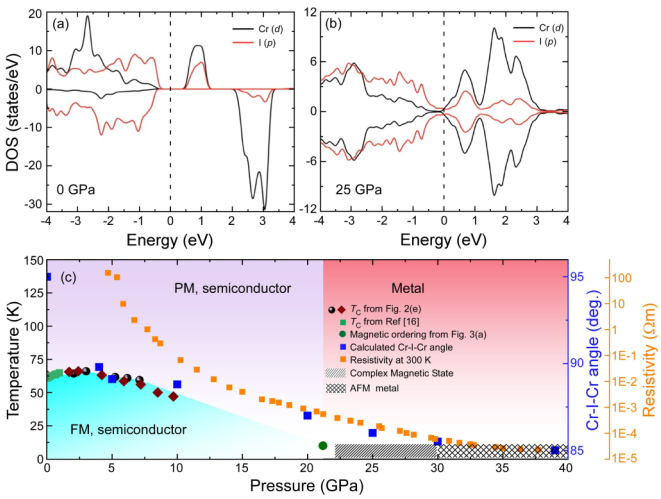

FIG. 4. Calculated density of states (DOS) showing the contributions of the up-spin (DOS >0) and down-spin (DOS <0) states in the Cr 3d and I 5p orbitals at (a) 0 GPa and (b) 25 GPa. A clear energy gap at 0 GPa reflects semiconducting character, whereas the gap disappears at 25 GPa signifying metallic character. (c) Pressure-temperature phase diagram of CrI_3, reflecting various magnetic and electronic phases. The highest T_c corresponds to the calculated Cr-I-Cr bond angle of 89.8° at 4 GPa, which satisfies the GKA rule. The low-temperature and high-pressure metallic phase between 22 and 30 GPa is designated as a complex magnetic state. The region above 30 GPa is marked as an AFM metallic state. PM, paramagnetic.

and the Cr-3d state in the conduction band, resulting in a band gap of 0.96 and 2.68 eV for the spin-up and spin-down electrons, respectively (see also Figs. S7 and S8). The projected density of states (PDOS) at 25 GPa [Fig. 4(b)] represents the electronic structure of an AFM coupling, with an onset of metallic character. This also corroborates the evolution of inverse temperature dependence of positive MR above 24 GPa [Fig. 3(c)] due to enhanced spin-spin scattering from the in-plane AFM spin orientation of the sample at low temperatures in the the resistivity measurements of Fig. 3(d).

Our calculations suggest a decrease in the Cr-I-Cr bond angle and Cr-I bond length with pressure. As a consequence, the magnetic ordering is highly suppressed in concurrence with a transition to a metallic phase at high pressure. All these high-pressure phases are summarized in the pressure-temperature phase diagram in Fig. 4(c). At ambient temperature, the resistivity decreases with pressure, resembling a pressure-induced transition to a metallic state. As pointed out in Fig. 3(d), we mark the metallic region above 22 GPa. The decrease in resistivity and T_c with increase in pressure occur concurrently, meaning that the magnetic ordering (primarily FM) exists in the semiconducting phase, below 21 GPa. Furthermore, in the metallic regime (above 22 GPa), the quenching of FM ordering at low temperature reflects a complex magnetic state [shaded region in Fig. 4(c)] that requires further measurements to be identified more precisely. We note, however, that the calculated Heisenberg exchange parameters, discussed in the Supplemental Material [17], are entirely consistent with a state right in the middle between a FM and AFM configuration. In fact, the exchange parameters shown in Fig. S6 are very similar to the exchange parameters of the so-called self-induced spin glass of elemental Nd [56]. If this also holds true for CrI_3, it would demonstrate that self-induced spin-glass states are not just found for isolated systems, or elements, but can in fact be found in a wider range of systems. At pressures above 30 GPa, theory and experiment point to a regular antiferromagnetic, metallic state of CrI_3.

To summarize, we have mapped out a pressure-temperature phase diagram of CrI_3 up to 40 GPa. We observe, from combined advanced experimental and theoretical investigations, a pressure-induced semiconductor-to-metal transition that is accompanied by a transition from a robust FM state to gradually more dominating AFM interactions in the metallic state. This makes CrI_3 a rather unique material, since normally such electronic transitions show exactly the opposite trend (AFM interactions turning FM). From spin-polarized DFT, we reveal a decrease in the Cr-I-Cr bond angle from 95° at ambient pressure to 85° at 25 GPa. The pressure-induced variation in the bond angle affects the FM superexchange interaction and leads to the nonmonotonic variation in the T_c with pressure. The quenching of FM ordering temperature, observed here, represents a complex magnetic state at low temperature and high pressure, in agreement with the theoretical data presented here. Our electronic structure calculations support the experimental observations and show the emergence of a finite DOS, primarily contributed by the Cr-3d states, at the Fermi level at and above 25 GPa. The present study will therefore open up possibilities of extensive research to explore the low-temperature, high-pressure metallic phase and further calculations of CrI_3 and similar 2D materials.

ACKNOWLEDGMENTS

A.G. and M.A.-H. acknowledge financial support from the Carl Tryggers Foundation and the Swedish Research Council (VR) under Project No. 2018-05393. Support by the P220 291 program of the Government of Russia through Project No. 292 075-15-2021-604 and President of Russia through Project No. NSh-2394.2022.1.5 is acknowledged. G.H. and M.K. acknowledge support from the Czech Science Foundation (Project No. 20-08633X). J.V. acknowledges the support of Czech Research Infrastructures MGML (Project No. LM2018096). O.E. acknowledges financial support from the Knut and Alice Wallenberg Foundation, eSSENCE, SNIC, the VR, the Foundation for Strategic Research (SSF), and the ERC (Synergy Grant FASTCORR, Project No. 854843). Y.K. acknowledges financial support from the VR under Project No. 2019-03569. The computations and data handling were enabled by resources provided by the Swedish National Infrastructure for Computing (SNIC), partially funded by the Swedish Research Council through Grant Agreement No. 2018-05973.

[1] K. S. Novoselov, A. Mishchenko, A. Carvalho, and A. H. Castro Neto, 2D materials and van der Waals heterostructures, Science **353**, 6298 (2016).

[2] C. Gong, L. Li, Z. Li, H. Ji, A. Stern, Y. Xia, T. Cao, W. Bao, C. Wang, Y. Wang, Z. Q. Qiu, R. J. Cava, S. G. Louie, J. Xia, and X. Zhang, Discovery of intrinsic ferromagnetism in two-dimensional van der Waals crystals, Nature (London) **546**, 265 (2017).

[3] M. Bonilla, S. Kolekar, Y. Ma, H. C. Diaz, V. Kalappattil, R. Das, T. Eggers, H. R. Gutierrez, M. H. Phan, and M. Batzill, Strong room-temperature ferromagnetism in VSe_2 monolayers on van der Waals substrates, Nat. Nanotechnol. **13**, 289 (2018).

[4] B. Huang, G. Clark, E. Navarro-Moratalla, D. R. Klein, R. Cheng, K. L. Seyler, Di. Zhong, E. Schmidgall, M. A. McGuire, D. H. Cobden, W. Yao, D. Xiao, P. Jarillo-Herrero, and X. Xu, Layer-dependent ferromagnetism in a van der Waals crystal down to the monolayer limit, Nature (London) **546**, 270 (2017).

[5] L. Thiel, Z. Wang, M. A. Tschudin, D. Rohner, I. Gutierrez-Lezama, N. Ubrig, M. Gibertini, E. Giannini, A. F. Morpurgo, and P. Maletinsky, Probing magnetism in 2D materials at the nanoscale with single-spin microscopy, Science **364**, 973 (2019).

[6] N. D. Mermin and H. Wagner, Absence of Ferromagnetism or Antiferromagnetism in One- or Two-Dimensional Isotropic Heisenberg Models, Phys. Rev. Lett. **17**, 1133 (1966).

[7] O. Besbes, S. Nikolaev, N. Meskini, and I. Solovyev, Microscopic origin of ferromagnetism in the trihalides $CrCl_3$ and CrI_3, Phys. Rev. B **99**, 104432 (2019).

[8] D. H. Kim, K. Kim, K. T. Ko, J. Seo, J. S. Kim, T. H. Jang, Y. Kim, J. Y. Kim, S. W. Cheong, and J. H. Park, Giant Magnetic Anisotropy Induced by Ligand LS Coupling in Layered Cr Compounds, Phys. Rev. Lett. **122**, 207201 (2019).

[9] S. W. Jang, M. Y. Jeong, H. Yoon, S. Ryee, and M. J. Han, Microscopic understanding of magnetic interactions in bilayer CrI_3, Phys. Rev. Mater. **3**, 031001(R) (2019).

[10] J. L. Lado and J. Fernandez-Rossier, On the origin of magnetic anisotropy in two dimensional CrI_3, 2D Mater. **4**, 035002 (2017).

[11] A. Frisk, L. B. Duffy, S. Zhang, G. van der Laan, and T. Hesjedal, Magnetic x-ray spectroscopy of two-dimensional CrI_3 layers, Mater. Lett. **232**, 5 (2018).

[12] J. Kanamori, Superexchange interaction and symmetry properties of electron orbitals, J. Phys. Chem. Solids **10**, 87 (1959).

[13] L. Webster and J. A. Yan, Strain-tunable magnetic anisotropy in monolayer $CrICl_3$, $CrBr_3$, and CrI_3, Phys. Rev. B **98**, 144411 (2018).

[14] Z. Wu, J. Yu, and S. Yuan, Strain-tunable magnetic and electronic properties of monolayer CrI_3, Phys. Chem. Chem. Phys. **21**, 7750 (2019).

[15] M. Pizzochero and O. V. Yazyev, Inducing magnetic phase transitions in monolayer CrI_3 via lattice deformations, J. Phys. Chem. C **124**, 7585 (2020).

[16] S. Mondal, M. Kannan, M. Das, L. Govindaraj, R. Singha, B. Satpati, S. Arumugam, and P. Mandal, Effect of hydrostatic pressure on ferromagnetism in two-dimensional CrI_3, Phys. Rev. B **99**, 180407(R) (2019).

[17] See Supplemental Material at http://link.aps.org/supplemental/10.1103/PhysRevB.105.L081104 for the experimental and calculation details and the supporting results.

[18] A. K. Arora, M. Rajalakshmi, T. R. Ravindran, and V. Sivasubramanian, Raman spectroscopy of optical phonon confinement in nanostructured materials, J. Raman Spectrosc. **38**, 604 (2007).

[19] T. Li, S. Jiang, N. Sivadas, Z. Wang, Y. Xu, D. Weber, J. E. Goldberger, K. Watanabe, T. Taniguchi, C. J. Fennie, K. F. Mak, and J. Shan, Pressure-controlled interlayer magnetism in atomically thin CrI_3, Nat. Mater. **18**, 1303 (2019).

[20] G. Kresse and D. Joubert, From ultrasoft pseudopotentials to the projector augmented-wave method, Phys. Rev. B **59**, 1758 (1999).

[21] G. Kresse and J. Furthmüller, Efficiency of ab-initio total energy calculations for metals and semiconductors using a plane-wave basis set, Comput. Mater. Sci. **6**, 15 (1996).

[22] J. P. Perdew, K. Burke, and M. Ernzerhof, Generalized Gradient Approximation Made Simple, Phys. Rev. Lett. **77**, 3865 (1996).

[23] S. Grimme, J. Antony, S. Ehrlich, and H. Krieg, A consistent and accurate *ab initio* parametrization of density functional dispersion correction (DFT-D) for the 94 elements H-Pu, J. Chem. Phys. **132**, 154104 (2010).

[24] J. M. Wills, M. Alouani, P. Andersson, A. Delin, O. Eriksson, and O. Grechnyev, *Full-Potential Electronic Structure Method: Energy and Force Calculations with Density Functional and Dynamical Mean Field Theory* (Springer, Berlin, 2013).

[25] V. I. Anisimov, J. Zaanen, and O. K. Andersen, Band theory and Mott insulators: Hubbard *U* instead of Stoner I, Phys. Rev. B **44**, 943 (1991).

[26] P. Jiang, C. Wang, D. Chen, Z. Zhong, Z. Yuan, Z. Y. Lu, and W. Ji, Stacking tunable interlayer magnetism in bilayer CrI_3, Phys. Rev. B **99**, 144401 (2019).

[27] Y. O. Kvashnin, A. Bergman, A. I. Lichtenstein, and M. I. Katsnelson, Relativistic exchange interactions in CrX_3 (X = Cl, Br, I) monolayers, Phys. Rev. B **102**, 115162 (2020).

[28] W. B. Zhang, Q. Qu, P. Zhu, and C. H. Lam, Robust intrinsic ferromagnetism and half semiconductivity in stable two-dimensional single-layer chromium trihalides, J. Mater. Chem. C **3**, 12457 (2015).

[29] M. Pizzochero, R. Yadav, and O. V. Yazyev, Magnetic exchange interactions in monolayer CrI_3 from many-body wavefunction calculations, 2D Mater. **7**, 035005 (2020).

[30] M. Dupont, Y. O. Kvashnin, M. Shiranzaei, J. Fransson, N. Laflorencie, and A. Kantian, Monolayer $CrCl_3$, an Ideal Test Bed for the Universality Classes of 2D Magnetism, Phys. Rev. Lett. **127**, 037204 (2021).

[31] N. Sivadas, S. Okamoto, X. Xu, C. J. Fennie, and D. Xiao, Stacking-dependent magnetism in bilayer CrI_3, Nano Lett. **18**, 7658 (2018).

[32] A. Majumdar, D. VanGennep, J. Brisbois, D. Chareev, A. V. Sadakov, A. S. Usoltsev, M. Mito, A. V. Silhanek, T. Sarkar, A. Hassan, O. Karis, R. Ahuja, and M. Abdel-Hafiez, Interplay of charge density wave and multiband superconductivity in layered quasi-two-dimensional materials: The case of 2H-NbS_2 and 2H-$NbSe_2$, Phys. Rev. Mater. **4**, 084005 (2020).

[33] M. Abdel-Hafiez, M. Mito, K. Shibayama, S. Takagi, M. Ishizuka, A. N. Vasiliev, C. Krellner, and H. K. Mao, High-pressure phase diagram of $NdFeAsO_{0.9}F_{0.1}$: Disappearance of superconductivity on the verge of ferromagnetism from Nd moments, Phys. Rev. B **98**, 094504 (2018).

[34] Y. Kvashnin, D. Vangennep, M. Mito, S. A. Medvedev, R. Thiyagarajan, O. Karis, A. N. Vasiliev, O. Eriksson, and M. Abdel-Hafiez, Coexistence of Superconductivity and Charge Density Waves in Tantalum Disulfide: Experiment and Theory, Phys. Rev. Lett. **125**, 186401 (2020).

[35] M. Abdel-Hafiez, X. M. Zhao, A. A. Kordyuk, Y.-W. Fang, B. Pan, Z. He, C.-G. Duan, J. Zhao, and X. J. Chen, Enhancement of superconductivity under pressure and the magnetic phase diagram of tantalum disulfide single crystals, Sci. Rep. **6**, 31824 (2016).

[36] A. McCreary, T. T. Mai, F. G. Utermohlen, J. R. Simpson, K. F. Garrity, X. Feng, D. Shcherbakov, Y. Zhu, J. Hu, D. Weber, K. Watanabe, T. Taniguchi, J. E. Goldberger, Z. Mao, C. N. Lau, Y. Lu, N. Trivedi, R. Valdés Aguilar, and A. R. Hight Walker, Distinct magneto-Raman signatures of spin-flip phase transitions in CrI_3, Nat. Commun. **11**, 3879 (2020).

[37] T. Song, Z. Fei, M. Yankowitz, Z. Lin, Q. Jiang, K. Hwangbo, Q. Zhang, B. Sun, T. Taniguchi, K. Watanabe, M. A. McGuire, D. Graf, T. Cao, J. H. Chu, D. H. Cobden, C. R. Dean, D. Xiao, and X. Xu, Switching 2D magnetic states via pressure tuning of layer stacking, Nat. Mater. **18**, 1298 (2019).

[38] Z. Wang, I. Gutiérrez-Lezama, N. Ubrig, M. Kroner, M. Gibertini, T. Taniguchi, K. Watanabe, A. Imamoğlu, E. Giannini, and A. F. Morpurgo, Very large tunneling magnetoresistance in layered magnetic semiconductor CrI_3, Nat. Commun. **9**, 2516 (2018).

[39] K. Mathew, R. Sundararaman, K. Letchworth-Weaver, T. A. Arias, and R. G. Hennig, Implicit solvation model for density-functional study of nanocrystal surfaces and reaction pathways, J. Chem. Phys. **140**, 084106 (2014).

[40] J. P. Perdew, M. Ernzerhof, and K. Burke, Rationale for mixing exact exchange with density functional approximations, J. Chem. Phys. **105**, 9982 (1996).

[41] G. Kresse and J. Furthmüller, Efficient iterative schemes for *ab initio* total-energy calculations using a plane-wave basis set, Phys. Rev. B **54**, 11169 (1996).

[42] F. Han, Projector-augmented plane-wave method, in *Problems in Solid State Physics with Solutions* (World Scientific, Singapore, 2011), Chap. 23, p. 391.

[43] H. J. Monkhorst and J. D. Pack, Special points for Brillouin-zone integrations, Phys. Rev. B **13**, 5188 (1976).

[44] A. I. Liechtenstein, V. I. Anisimov, and J. Zaanen, Density-functional theory and strong interactions: Orbital ordering in Mott-Hubbard insulators, Phys. Rev. B **52**, R5467(R) (1995).

[45] S. L. Dudarev, G. A. Botton, S. Y. Savrasov, Z. Szotek, W. M. Temmerman, and A. P. Sutton, Electronic structure and elastic properties of strongly correlated metal oxides from first principles: LSDA + U, SIC-LSDA and EELS study of UO_2 and NiO, Phys. Status Solidi A **166**, 429 (1999).

[46] M. A. McGuire, H. Dixit, V. R. Cooper, and B. C. Sales, Coupling of crystal structure and magnetism in the layered, ferromagnetic insulator CrI_3, Chem. Mater. **27**, 612 (2015).

[47] D. T. Larson and E. Kaxiras, Raman spectrum of CrI_3: An *ab initio* study, Phys. Rev. B **98**, 085406 (2018).

[48] S. Djurdjic-Mijin, A. Šolajic, J. Pešic, M. Šcepanovic, Y. Liu, A. Baum, C. Petrovic, N. Lazarevic, and Z. V. Popovic, Lattice dynamics and phase transition in CrI_3 single crystals, Phys. Rev. B **98**, 104307 (2018).

[49] W. Jin, Z. Ye, X. Luo, B. Yang, G. Ye, F. Yin, H. H. Kim, L. Rojas, S. Tian, Y. Fu, S. Yan, H. Lei, K. Sun, A. W. Tsen, R. He, and L. Zhao, Tunable layered-magnetism-assisted magneto-Raman effect in a two-dimensional magnet CrI_3, Proc. Natl. Acad. Sci. USA **117**, 24664 (2020).

[50] P. Nordblad, *Disordered magnetic systems*, in *Reference Module in Materials Science and Materials Engineering* (Elsevier, New York, 2016).

[51] X. Ke, M. L. Dahlberg, E. Morosan, J. A. Fleitman, R. J. Cava, and P. Schiffer, Magnetothermodynamics of the Ising antiferromagnet $Dy_2Ge_2O_7$, Phys. Rev. B **78**, 104411 (2008).

[52] D. R. Klein, D. MacNeill, J. L. Lado, D. Soriano, E. Navarro-Moratalla, K. Watanabe, T. Taniguchi, S. Manni, P. Canfield, J. Fernandez-Rossier, and P. Jarillo-Herrero, Probing magnetism in 2D van der Waals crystalline insulators via electron tunneling, Science **360**, 1218 (2018).

[53] T. Song, X. Cai, M. W. Y. Tu, X. Zhang, B. Huang, N. P. Wilson, K. L. Seyler, L. Zhu, T. Taniguchi, K. Watanabe, M. A. McGuire, D. H. Cobden, D. Xiao, W. Yao, and X. Xu, Giant tunneling magnetoresistance in spin-filter van der Waals heterostructures, Science **360**, 1214 (2018).

[54] *Spintronics for Next Generation Innovative Devices*, edited by K. Sato and E. Saitoh (Wiley, New York, 2015).

[55] N. Ali and S. B. Woods, Magnetoresistance of antiferromagnetic metals with localized magnetic moments, J. Appl. Phys. (Melville, NY) **61**, 4393 (1987).

[56] U. Kamber, A. Bergman, A. Eich, D. Iuşan, M. Steinbrecher, N. Hauptmann, L. Nordström, M. I. Katsnelson, D. Wegner, O. Eriksson, and A. A. Khajetoorians, Self-induced spin glass state in elemental and crystalline neodymium, Science **368**, eaay6757 (2020).

[57] L. Chen, J. Chung, B. Gao, T. Chen, M. B. Stone, A. I. Kolesnikov, Q. Huang, and P. Dai, Topological Spin Excitations in Honeycomb Ferromagnet CrI_3, Phys. Rev. X **8**, 041028 (2018).